

# Journal of Biomedical Optics

BiomedicalOptics.SPIEDigitalLibrary.org

## **Spectral wide-field microscopic fluorescence resonance energy transfer imaging in live cells**

Lili Zhang  
Guiqi Qin  
Liuying Chai  
Jiang Zhang  
Fangfang Yang  
Hongqin Yang  
Shusen Xie  
Tongsheng Chen

# Spectral wide-field microscopic fluorescence resonance energy transfer imaging in live cells

Lili Zhang,<sup>a</sup> Guiqi Qin,<sup>a</sup> Liuying Chai,<sup>a</sup> Jiang Zhang,<sup>a</sup> Fangfang Yang,<sup>a</sup> Hongqin Yang,<sup>b</sup> Shusen Xie,<sup>b,\*</sup> and Tongsheng Chen<sup>a,\*</sup>

<sup>a</sup>South China Normal University, College of Life Science, MOE Key Laboratory of Laser Life Science and Institute of Laser Life Science, Guangzhou 510631, China

<sup>b</sup>Fujian Normal University, Institute of Laser and Optoelectronics Technology, Key Laboratory of Optoelectronic Science and Technology for Medicine of Ministry of Education, Fuzhou 350007, China

**Abstract.** With its precise, sensitive, and nondestructive features, spectral unmixing-based fluorescence resonance energy transfer (FRET) microscopy has been widely applied to visualize intracellular biological events. In this report, we set up a spectral wide-field microscopic FRET imaging system by integrating a varispec liquid crystal tunable filter into a wide-field microscope for quantitative FRET measurement in living cells. We implemented a representative emission-spectral unmixing-based FRET measurement method on this platform to simultaneously acquire pixel-to-pixel images of both FRET efficiency ( $E$ ) and acceptor-to-donor concentration ratio ( $R_C$ ) in living HepG2 cells expressing fusion proteins in the presence or absence of free donors and acceptors and obtained consistent results with other instruments and methods. This stable and low-cost spectral wide-field microscopic FRET imaging system provides a new toolbox for imaging molecular events with high spatial resolution in living cells. © 2015 Society of Photo-Optical Instrumentation Engineers (SPIE) [DOI: 10.1117/1.JBO.20.8.086011]

Keywords: fluorescence resonance energy transfer; quantitative imaging; wide-field microscope; spectral unmixing; varispec liquid crystal tunable filter; living cells.

Paper 150273R received Apr. 30, 2015; accepted for publication Jul. 21, 2015; published online Aug. 17, 2015.

## 1 Introduction

Fluorescence resonance energy transfer (FRET) has been extensively applied to visualize the fundamental physicochemical processes of molecular binding, association, conformation change, diffusion, and catalysis in living cells.<sup>1,2</sup> Famous as a “nanoruler,” 1 to 20 nm of dynamic spatial range is just the biological scale of intramolecular and intermolecular distances.<sup>3–5</sup> Genetically encoded fluorescent proteins (FPs)-based biosensors make FRET technology capable of resolving dynamic signaling events inside living cells without influencing normal physiological activities.<sup>6</sup> Microscopic FRET imaging can visualize subcellular temporal-spatial processes *in situ*.<sup>7,8</sup>

Sensitized emission-based FRET quantification, the most widely used FRET imaging approach for dynamic FRET applications in living cells, can be divided into two categories: three-cube method<sup>9,10</sup> and spectral unmixing method.<sup>11,12</sup> Recently, the three-cube method for two-fluorophore FRET quantification has been developed to resolve multicolor FRET signals with multicube combinations.<sup>13,14</sup> Spectral unmixing methods, including sRET,<sup>15</sup> lux-FRET,<sup>16</sup> SpRET,<sup>12</sup> Iem-spFRET,<sup>17</sup> and ExEm spectral unmixing,<sup>18</sup> have growing impacts on FRET quantification with substantially enhanced precision and sensitivity compared to the cube method.

Spectral unmixing-based FRET imaging is commonly implemented on confocal microscope with spectral detectors.<sup>12,15,17,18</sup> Accurate calibration of instrument is a prerequisite for quantitative FRET measurement.<sup>12,16</sup> Although a confocal microscope is characterized by highly automated operation, its status is

mutable, and the correction coefficients for FRET quantification depend on fluorescence intensity or FPs' expression levels that vary largely among cells.<sup>19–21</sup> Hence, rigorous system calibration and signal correction are generally needed for almost every quantitative FRET measurement with a confocal microscope, which is very tedious and difficult even for the experts on live-cell FRET application.<sup>21</sup> In contrast to confocal microscope, previous reports and our studies have shown that the status and performance of wide-field microscopes are quite stable for at least 3 months.<sup>11,19–21</sup> However, to our knowledge, there is no report about spectral unmixing-based live-cell FRET imaging on wide-field microscope, presumably due to the great challenge in simultaneously collecting a spatial fluorescence signal and spectral information.

In this study, we integrated a varispec liquid crystal tunable filter (LCTF) into a wide-field microscope to develop a spectral wide-field microscopic FRET imaging system for spectral unmixing-based quantitative FRET imaging in living cells. In order to verify this spectral wide-field FRET imaging system, we implemented a spectral unmixing FRET quantification method (Iem-spFRET) on our platform to acquire FRET efficiency ( $E$ ) and acceptor-to-donor concentration ratio ( $R_C$ ) images for fusion proteins in the absence or presence of free acceptors and donors in live HepG2 cells. This report provides a stable platform to perform a spectral unmixing-based FRET quantification method, which not only steps into the vacuum to implement spectral unmixing FRET imaging with a wide-field microscope but also takes the stability and low-cost of the platform into account.

\*Address all correspondence to: Shusen Xie, E-mail: [ssxie@fjnu.edu.cn](mailto:ssxie@fjnu.edu.cn); Tongsheng Chen, E-mail: [chentsh@sclu.edu.cn](mailto:chentsh@sclu.edu.cn) and [chentsh126@126.com](mailto:chentsh126@126.com)

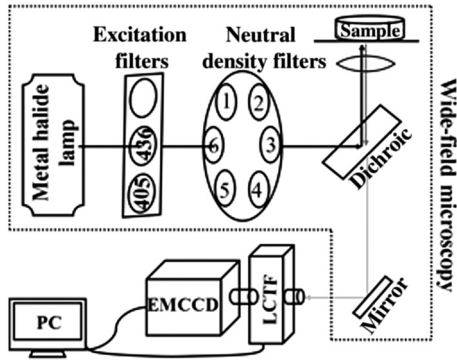


**Fig. 1** Illustration on the spectral wide-field microscopic fluorescence resonance energy transfer (FRET) imaging system.

## 2 Materials and Methods

### 2.1 Spectral Wide-Field Microscopic Fluorescence Resonance Energy Transfer Imaging System

Figure 1 depicts the schematic of our spectral wide-field microscopic FRET imaging system, which consists of a wide-field microscope (Axio Observer, Carl Zeiss, Oberkochen, Germany) and an LCTF (Varispec LCTF, VIS-10-20-STD, CRI, Cambridge), which bridges the emCCD (DU-897U-CS0-EXF, Andor, Belfast, England) and microscope with standard C ports.

The inverted wide-field fluorescence microscope is equipped with a metal halide lamp (X-Cite 120Q, Lumen Dynamics, California), a 40 $\times$  oil immersion 1.3 NA objective, a three-hole excitation filters' plan, a neutral density filters' wheel, and a dichroic mirror (455DCLP, Chroma). The excitation wavelength is alternatively selected with two bandpass excitation filters of 405/20 nm (405-nm excitation) and 436/20 nm (436-nm excitation) (Chroma) by pushing or pulling the mobilizable three-hole plan. The excitation intensity is controlled by switching different luminosities (0%, 12.5%, 25%, 50%, 100% of the total luminosity) of the metal halide lamp and/or turning the neutral density filters' wheel between different attenuation degrees (2%, 20%, 40%, 50%, 70%, 100%, from 6 to 1 in Fig. 1). The dichroic filter can reflect the shorter-wavelength excitation light and pass the longer-wavelength emission light of the sample.

The Varispec LCTF that we used has a wavelength range of 400 to 720 nm, bandwidths [full-width at half-maximum (FWHM)] of 10 nm, and tunable time resolution of 20 ms.

### 2.2 lem-spFRET Method

The lem-sp-FRET method was described in detail in our recent work,<sup>17</sup> and can be summarized as the following main steps and final equations: (1) calibration of imaging system with a standard lamp, (2) measurement of the emission spectral fingerprints of the donor [ $e_D(\lambda)$ ] and acceptor [ $e_A(\lambda)$ ], (3) determination of the extinction coefficient ratio ( $\gamma_i$ ) of acceptor to donor at each excitation wavelength  $i$  with a reference tandem sample according to

$$\gamma_i = \frac{1 - \Phi \delta_i E - E}{\Phi \delta_i}, \quad (1)$$

where  $\Phi$  is the theoretical fluorophore quantum yield ratio of the acceptor to donor,  $E$  is the FRET efficiency of the reference

tandem sample, which should be known or predetermined by another FRET quantification method, (4) acquiring spectra  $S(\lambda)$  of the FRET sample at each of two excitation wavelengths, (5) unmixing every spectrum with the fingerprints of the donor and acceptor as

$$S(\lambda) = \alpha \cdot e_D(\lambda) + \beta \cdot e_A(\lambda)$$

to determine the apparent concentration ratio of donor to acceptor:

$$\delta = \frac{\alpha}{\beta}, \quad (2)$$

and (6) calculating the  $E$  and  $R_C$  with the  $\gamma$  and  $\delta$  at two excitation wavelengths,

$$E = \frac{\delta_{436}\gamma_{436} - \delta_{405}\gamma_{405}}{\delta_{405}\delta_{436}(\gamma_{436} - \gamma_{405})\Phi + \delta_{436}\gamma_{436} - \delta_{405}\gamma_{405}}, \quad (3)$$

$$R_C = \frac{\delta_{405} - \delta_{436}}{\delta_{405}\delta_{436}(\gamma_{436} - \gamma_{405})\Phi + \delta_{436}\gamma_{436} - \delta_{405}\gamma_{405}}. \quad (4)$$

The subscripts of 405 and 436 denote the excitation wavelengths of 405 and 436 nm, respectively, used in this report.

### 2.3 Partial Acceptor Photobleaching-Based Fluorescence Resonance Energy Transfer Methods

Partial acceptor photobleaching-based FRET (PbFRET) quantification, a calibration-free method, was used as a reference method in this report.<sup>5,22</sup> PbFRET methods are usually implemented either by simultaneously detecting the fluorescence intensity in both the donor and acceptor channels at donor excitation or by separately determining the acceptor photobleaching degree  $x$  in the acceptor channel at a selective acceptor excitation and as the donor intensity increases by multiple  $R(x)$  in the selective donor detection channel at donor excitation before and after partially photobleaching the acceptors.<sup>22-24</sup> The latter implementation, put forward by Elder et al. (E-PbFRET) for a single-acceptor FRET construct,<sup>22</sup> has been perfectly developed to quantify the multiple-acceptor FRET construct by our group.<sup>5,25,26</sup>

For a one-acceptor FRET construct, according to E-PbFRET theory,<sup>22</sup> we can determine  $E$  with

$$E = \frac{R(x) - 1}{R(x) - 1 + x}. \quad (5)$$

For a multiple-acceptor FRET construct ( $1D \sim nA$ ,  $n$ -acceptor FRET construct), partially photobleaching acceptors of  $1D \sim nA$  constructs lead to a complicated system consisting of  $n + 1$  kinds of constructs, written as a general symbol  $(n - i)T \sim 1D \sim iA$  ( $i$ -acceptor FRET construct,  $T$  stands for the photobleached acceptor), with different FRET efficiencies  $E_i$  and proportions  $P_i(x) = C_i n(1 - x)^i x^{n-i}$  complying to binomial distribution theory. Then  $R(x)$  is a linear combination of  $P_i(x)$ :<sup>5</sup>

$$R(x) = \sum_{i=0}^n P_i(x) y_i, \quad (6)$$

where  $y_i = (1 - E_i)/(1 - E_n)$  are the linear proportional constants that can be acquired by fitting with the  $R(x)$  and  $x$  according to Eq. (5). Then  $E_n$  of the  $n$ -acceptor FRET constructs can be calculated with the first fitting constant  $y_0$ :

$$E_n = 1 - \frac{1}{y_0}. \quad (7)$$

## 2.4 Microscopic Imaging

For spectral imaging, 405- and 436-nm excitations were attenuated to 0.25%, 0.5%, or 1% according to the expression level of the FPs. Emission was scanned at a step resolution of 13 nm in the range of 464 to 607 nm for donor-only and acceptor-only samples or 464 to 555 nm for FRET samples with LCTF, and the corresponding 12/8 spectral images at each excitation were acquired with emCCD.

For E-PbFRET and Mb-PbFRET measurements,<sup>5,22</sup> a BP436/25-FT455-BP480/40 nm combination was used for donor (Cerulean) detection, a BP510/17-FT520-LP530 nm combination was used for acceptor (Venus) detection, and acceptors were selectively photobleached with a high intensity of excitation light selected with the BP 510/17-nm filter. emCCD was typically run in  $4 \times 4$  binning mode and the background (BG) was removed with the average reading the non-fluorescent cell area of each image.

## 2.5 Cell Culture, Transfection, and Plasmids

HepG2 cells, a human hepatocellular carcinoma cell line, were obtained from the Department of Medicine, Jinan University, Guangzhou, China. Cells were cultured in Dulbecco's modified Eagle's medium (DMEM, Gibco, Grand Island, New York) containing 10% fetal calf serum (FCS; Sijiqing, Hangzhou, China) at 37°C under 5% CO<sub>2</sub> in a humidified incubator.

For transfection, cells were cultured in DMEM containing 10% FCS in a 35-mm glass dish with a density of  $4 \times 10^4$  cells/ml at 37°C under 5% CO<sub>2</sub> in a humidified incubator. After 24 h, when the cells reached 70% to 90% confluence, plasmid was transfected into the HepG2 cells for 24 to 48 h. Lipofectamine 2000 (Invitrogen, Carlsbad) was used as a transfection reagent.

Cerulean (C, donor) and Venus (V, acceptor)-Kras plasmids were purchased from Addgene Company (Cambridge, Massachusetts). The FRET-standard constructs, including C-TRAF-Venus (CTV, the TRAF is a tumor necrosis factor receptor-associated factor domain including 229 amino acid), Cerulean-32-Venus, (C32V, Addgene plasmid 29396), Cerulean-5-Venus-5-Cerulean (CVC, Addgene plasmid 27788), and Venus-5-Cerulean-5-Venus (VCV, Addgene plasmid 27788), were kindly provided by the Vogel lab (National Institutes of Health, Bethesda, Maryland).<sup>15,27</sup>

## 3 Results and Discussion

### 3.1 Calibration and Spectral Fingerprints

Photobleaching of fluorophores during spectral imaging should be rigorously controlled for quantitative FRET measurement on our spectral wide-field imaging system. Figure 2(a) showed the representative time-lapse images of a living HepG2 cell expressing C32V with 1%, the strongest excitation intensity in our all experiments, of 436-nm excitation. The constant fluorescence

intensities of five living cells expressing C32V with 1% of 436-nm excitation during time-lapse imaging indicated a negligible photobleaching [Fig. 2(b)]. Photobleaching was also negligible in our experiments with 1% of 405-nm excitation (data not shown) due to lower extinction coefficients of both Cerulean and Venus at 405 nm than that at 436 nm.<sup>28</sup>

Rigorous spectral-sensitivity calibration of the instrument is the premise of accurate measurement for Iem-spFRET. We calibrated our spectral wide-field microscopic imaging system with a standard calibration light source (CLS, LS-1-CAL, Ocean Optics, Florida) that was placed on the objective, taking the place of samples to acquire the spectral images of CLS [Fig. 2(c), second row] when the light was on and the BG [Fig. 2(c), first row] when the light was off. Figure 2(d) showed standard CLS spectrum (National Institute of Standards and Technology) and measured CLS spectrum obtained by subtracting BG [Fig. 2(c), first row] from CLS [Fig. 2(c), second row], as well as the spectral response of our spectral wide-field microscopic imaging system. Throughout the paper, all spectra were calibrated with the response function in Fig. 2(d).

The 405- and 436-nm excitations on our spectral wide-field microscopic imaging system share the same dichroic mirror, wavelength range, and emCCD. Therefore, our system with each of the two excitations has the same response function, which largely improves the accuracy of the response measurements compared to the usually used different dichroic mirrors for different excitation wavelengths.<sup>12</sup> In addition, the quantum efficiency of emCCD that we used in the wavelength range of 464 to 607 nm is larger than 85%, making our system very sensitive even for dim light. Moreover, the high sensitivity of our system can be directly calibrated with the precalibrated CLS, which largely simplifies the operation and, in turn, improves the accuracy of instrument calibration compared to the calibration with a high power light source that should be precalibrated with CLS.<sup>11,17</sup> In fact, the calibration step is not mandatory for every measurement as our spectral wide-field microscope is very stable in a relatively long time period and we only need to calibrate it periodically.

Living HepG2 cells exclusively expressing Cerulean or Venus-Kras plasmid were used to obtain the spectral fingerprints of donors and acceptors. Figure 2(c) showed the representative spectral images of donor [Fig. 2(c), third row] and acceptors [Fig. 2(c), fourth row] directly acquired from our spectral wide-field imaging system at 436 nm excitation and Fig. 2(e) showed the fingerprints normalized to the unit area of Cerulean [ $e_D(\lambda)$ ] and Venus [ $e_A(\lambda)$ ] in living HepG2 cells from 10 frames.

In reality, the spectral fingerprints of donor and acceptor are independent of the instrument and illumination; thus, they can also be obtained with other instruments such as a spectrofluorometer.<sup>16</sup> Moreover, once the fingerprints were determined, we need not measure them for every experiment in a specific cell line. In order to insure accurate spectral unmixing, the wavelength range of fingerprints should overlap well with the total donor and acceptor emission spectra. The spectral ranges chosen in this study fulfill this requirement [Fig. 2(e)].

### 3.2 Determination of $\gamma_{405}$ and $\gamma_{436}$

We used living HepG2 cells expressing CTV plasmid to measure  $\gamma_{405}$  and  $\gamma_{436}$  of Venus to Cerulean on our spectral wide-field microscopic imaging system through the following three steps: (1) measuring the FRET efficiency ( $E$ ) of CTV in living

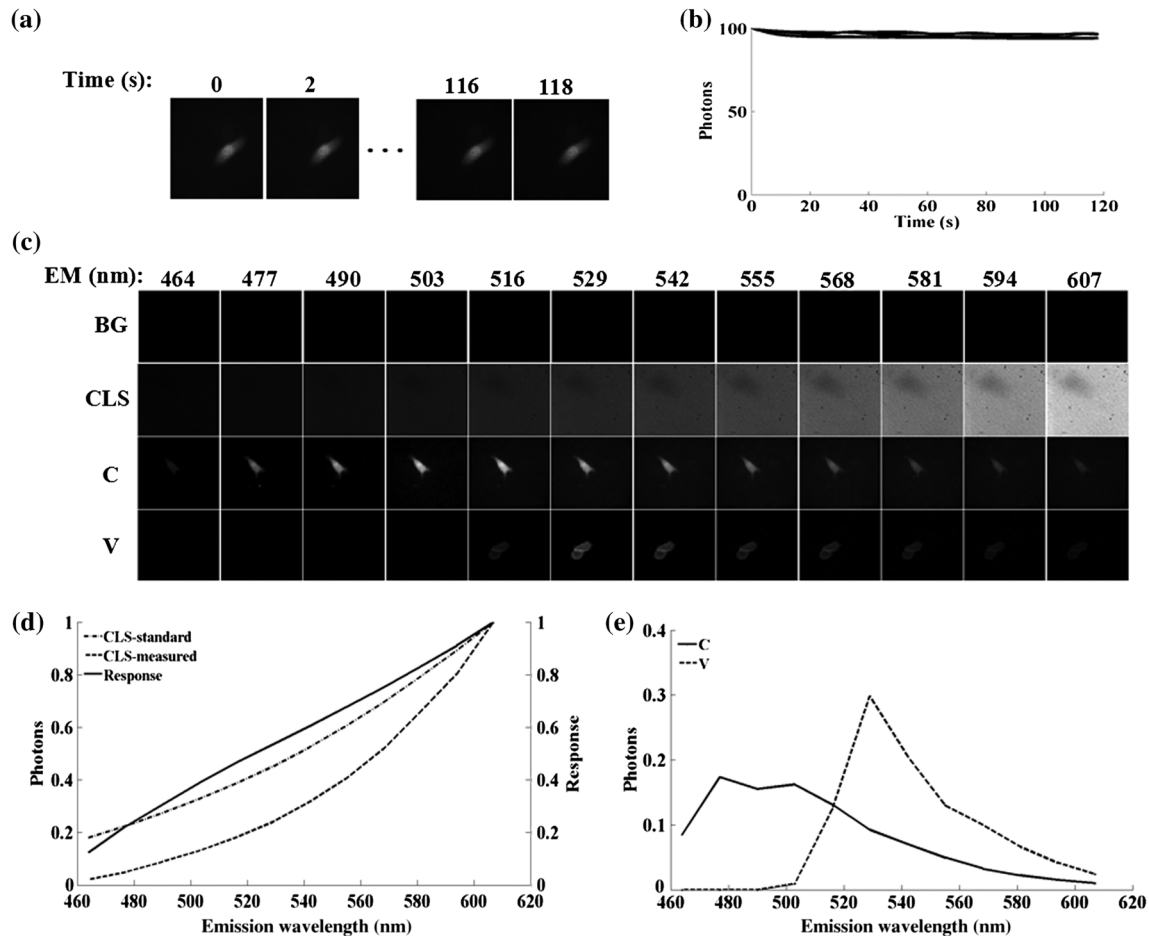


**Fig. 2** Calibration of the spectral wide-field imaging system and spectral fingerprints of donor (Cerulean) and acceptor (Venus) in living cells. (a) Time-lapse images of a living HepG2 cell expressing C32V with 436-nm excitation. (b) Dynamics of fluorescence intensity during time-lapse imaging. (c) Spectral images of background (BG), calibration light source (CLS), Cerulean (C) and Venus-Kras (V). (d) Spectral response of the spectral wide-field imaging system. (e) Normalized calibrated fingerprints of donor and acceptor.

HepG2 cells; (2) acquiring the spectra of living HepG2 cells expressing CTV with 405 and 436 nm excitation, respectively, to determine the  $\gamma_{405}$  and  $\gamma_{436}$  on our system according to Eq. (2); (3) calculation of  $\gamma_{405}$  and  $\gamma_{436}$  according to Eq. (1), where  $\Phi = 0.919$  is the quantum yield ratio of Venus (0.57) to Cerulean (0.62).<sup>29,30</sup> The  $E$  of CTV was measured with the E-PbFRET method. Figure 3(a) showed the representative fluorescence images of donors with a donor-filter combination before (D) and after (DP) partially photobleaching acceptors and that of acceptors with the acceptor-filter combination before (A) and after (AP) partially photobleaching acceptors of CTV. The corresponding pixel-to-pixel pseudo-color  $E$  image and histogram of living cells expressing CTV were also shown in Fig. 3(a). The  $E$  image was mostly blue mixed with some small areas of green, indicating a near zero  $E$  value and the corresponding histogram gave a peak value of 3.5% [Fig. 3(a)]. The average  $E$  of CTV measured by E-PbFRET method was  $4.3\% \pm 6.2\%$  ( $n = 25$ ), consistent with the results of  $6.3\% \pm 2.6\%$  measured by fluorescence lifetime imaging microscopy (FLIM), and  $1.7\% \pm 7.0\%$  measured by sRET in Vogel's laboratory.<sup>15</sup> The spectral images of living cells expressing FPs with 405- or 436-nm excitation were accordingly named as the  $S_{405}$  and  $S_{436}$  stacks throughout the article. Figure 3(b) showed the

representative  $S_{405}$  and  $S_{436}$  stacks of living cell expressing CTV, Fig. 3(c) showed the corresponding pixel-to-pixel pseudo-color  $\gamma_{405}$  and  $\gamma_{436}$  images, and Fig. 3(d) showed their histograms, indicating a peak value of about 0.29 and 0.395, respectively. The average peak values of  $\gamma_{405}$  and  $\gamma_{436}$  of Venus to Cerulean in living HepG2 cells on our spectral wide-field microscopic imaging system were  $0.29 \pm 0.03$  and  $0.41 \pm 0.06$  from 15 histograms.

Extinction coefficient ratios of fluorophores depend not only on their absorption spectra that may be affected by the physiological environments, but also on the optical transmission properties of the instrument used.<sup>1,16</sup> Although predeterminations of the extinction coefficient ratios of fluorophores at two excitations are indispensable, this step is not necessary for every FRET measurement. Once  $\gamma_{405}$  and  $\gamma_{436}$  are determined, we need not measure them for subsequent FRET measurements for the specific cell lines and imaging system even when we change the emission optical path and/or detector, because they are independent of the emission properties of the imaging system, and only relate to the absorption spectra of the fluorophores and the excitation spectra intrinsic to the photophysical features of the excitation light source and the excitation transmission characteristics of imaging system.

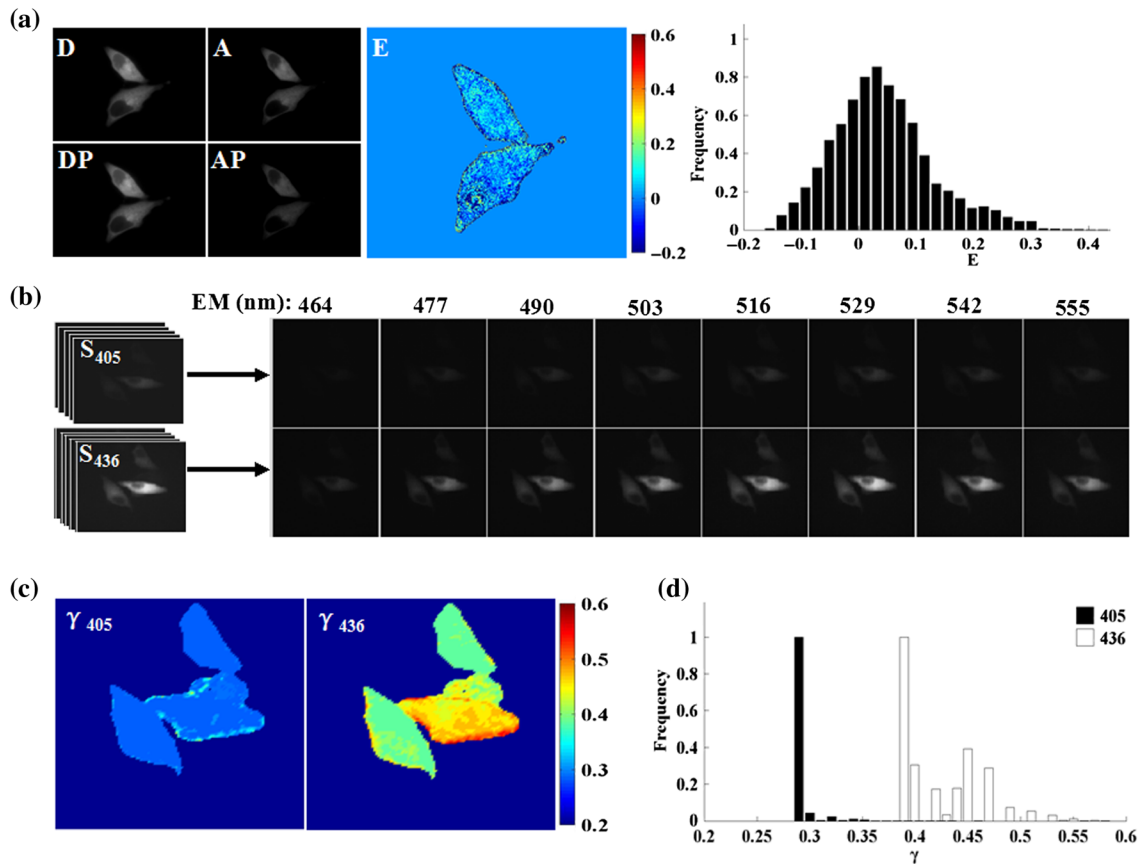


**Fig. 3** Extinction coefficient ratios of Venus to Cerulean at 405 ( $\gamma_{405}$ ) and 436 ( $\gamma_{436}$ ) nm in living HepG2 cells on our spectral wide-field microscopic FRET imaging system. (a) Representative pixel-to-pixel FRET efficiency ( $E$ ) images (left) and corresponding histogram of living cells expressing CTV measured by E-PbFRET method (right). (b) Representative spectral image-stacks of living cells expressing CTV with 405 ( $S_{405}$ ) and 436 nm ( $S_{436}$ ) excitation, respectively. (c)  $\gamma_{405}$  and  $\gamma_{436}$  images, and (d) the corresponding histograms of  $\gamma_{405}$  and  $\gamma_{436}$ .

### 3.3 Evaluation of the Spectral Wide-Field Microscopic System for Quantitative Fluorescence Resonance Energy Transfer Imaging

To evaluate our spectral wide-field microscopic FRET imaging system, we implemented Iem-spFRET method on this system to measure the  $E$  and  $R_C$  values of C32V, CVC, and VCV constructs inside living HepG2 cells. Figure 4 showed their representative  $S_{405}$  and  $S_{436}$  stacks [Fig. 4(a)], emission spectra normalized to the unit area [Fig. 4(b)], and the corresponding pixel-to-pixel pseudocolor  $E$  [Fig. 4(c), top row] and  $R_C$  [Fig. 4(c), bottom row] images as well as their histograms [Fig. 4(d)]. Two characteristics can be concluded from Fig. 4 (b): (1) Spectra had a higher emission at the acceptor's peak wavelength largely due to the energy transfer; (2) spectra with the 405-nm excitation had a higher donor peak and a lower acceptor peak than that with the 436-nm excitation due to  $\gamma_{405} < \gamma_{436}$ .  $E$  histograms exhibited the peaks of  $\sim 30\%$  for C32V and  $\sim 45\%$  for CVC as well as  $\sim 65\%$  for VCV [Figs. 4(c) and 4(d), top row]. The statistical  $E$  values from 10 frames were  $31.3\% \pm 3.3\%$  for C32V and  $68.24 \pm 6.4\%$  for VCV, consistent with the  $E$  values of  $28.2 \pm 4.1\%$  and  $66.3\% \pm 1.4\%$  for C32V measured by E-PbFRET and VCV measured by Mb-PbFRET. Cells expressing CVC from six

frames had an average  $E$  value of  $46.8\% \pm 5.1\%$ , very consistent value measured by Vogel's laboratory with FLIM and sRET methods.<sup>15,31</sup> The corresponding  $R_C$  histograms revealed their concentration ratio between Venus and Cerulean:  $\sim 0.98$  for C32V,  $\sim 0.50$  for CVC, and  $\sim 1.95$  for VCV [Fig. 4(c), bottom row]. The statistical  $R_C$  peaks from at least six frames were  $0.98 \pm 0.05$  for C32V,  $0.52 \pm 0.27$  for CVC, and  $2.03 \pm 0.78$  for VCV, in agreement with the corresponding theoretical values of 1, 0.5, and 2.

In principle, spectral unmixing-based FRET quantification methods including sRET,<sup>15</sup> SpRET,<sup>12</sup> and lux-FRET<sup>16</sup> can also be implemented on our spectral wide-field microscopic imaging system. In reality, lux-FRET had been successfully implemented on our wide-field microscopic FRET system to measure the  $E$  values of constructs in single living cells (data not shown). In addition, this spectral wide-field microscopic FRET imaging system can be developed to implement excitation-emission (ExEm) spectral unmixing-based FRET method<sup>18</sup> and multi-color FRET imaging<sup>13,14</sup> by adding appropriate excitation filters and dichroic mirrors, which has been experimentally completed by our group and we will publish these data in the near future.

We note that some pixels in the pseudocolor maps present abnormal  $E$  or  $R_C$  values [Fig. 4(c)], which may be due to the long detection time for the spectral image-stacks. Our spectral wide-field imaging system is still in the stage of completely

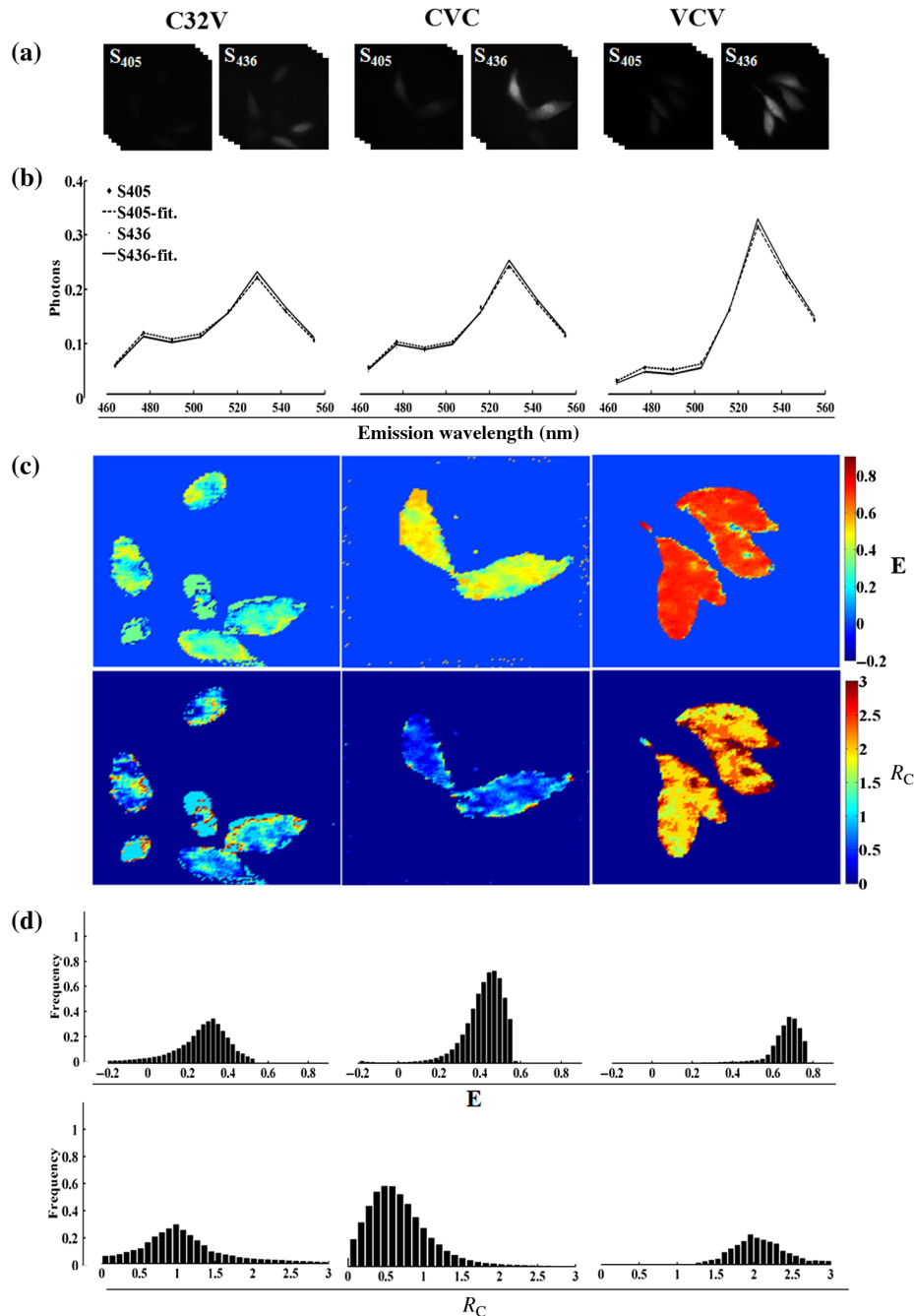


**Fig. 4** Implementation of lem-spFRET on the spectral wide-field microscopic imaging system. (a) Representative  $S_{405}$  and  $S_{436}$  stacks. (b) Representative spectra with 405- or 436-nm excitation. (c) Pixel-to-pixel  $E$  and  $R_C$  images of living HepG2 cells expressing C32V, CVC and VCV, respectively, and (d) the corresponding histograms of  $E$  and  $R_C$  pixel values.

manual operation. By considering exact match of the spectral images to the emission wavelength scanned by the Varispec LCTF, we chose a relative long exposure time of 300 to 1000 ms for imaging, and a time interval of 2000 ms for both time-lapse detection and LCTF wavelength scanning. The entire process to acquire  $S_{405}$  and  $S_{436}$  stacks including the interval between two excitation wavelengths switching takes about 50 s, which was a relatively long time for molecular mobility in living cells and noise variability of emCCD as well as power stability of the excitation light source. These problems would be greatly weakened if the spectral wide-field imaging

system could be electric controlled and automatically matched, which is currently under our research.

$E$  and  $R_C$  histograms of fusion FRET proteins with specific stoichiometry and distance between acceptor and donor exhibit a wide distribution [Fig. 4(d)], and similar reports have been published recently,<sup>12,15</sup> which may largely owe to the randomness of protein expression level in living cells. Although donor and acceptor DNA fragments are linked with fixed amino acids, they are still able to transcribe and translate independently. Hence, the inconsistent expression of donor and acceptor DNA fragments would lead to distributions of both  $E$  and

$R_C$  deviating from the theoretical values. In addition, the mobility of fluorescent molecules in living cells described in above paragraph may also result in the distribution of both  $E$  and  $R_C$  values.

The LCTF consists of several cascaded stages of a Lyot birefringent filter that has been made tunable with the addition of a liquid crystal layer in each stage, and the narrow bandpass is obtained by using successive stages to suppress the out-of-band transmission of the previous stage.<sup>32</sup> Thus, LCTF acts like a filter wheel with a very large number of narrow bandpass filters, which have a high rejection ratio for out-of-band transmission.<sup>33</sup> Although LCTF is particularly designed for spectral scanning and has been widely used in many research fields, the low transmission rate in the range of 460 to 600 nm has hindered its use for FRET quantification.<sup>34</sup> With the development of relevant technology, increase of transmission rate in the range of 460 to 600 nm (LCTFs, Data Sheet)<sup>35</sup> makes LCTF be successfully used for our spectral wide-field microscopic FRET imaging system. However, the relatively low transmission rate of LCTF in the range of 460 to 480 nm wavelength range [Fig. 2(d)], just the peak of Cerulean, is still a hinder for high-quality spectral FRET imaging especially for the 405-nm excitation of FRET constructs with large  $E$  value [Fig. 2(d)]. Even so, it can be seen from our results that our spectral

wide-field imaging system can quantify FRET constructs with  $E$  as high as  $\sim 70\%$  [Fig. 4, last column]. Moreover, this issue can be greatly improved for GFP-YFP and YFP-mCherry as well as YFP-RFP pairs.

We here for the first time performed a spectral unmixing-based FRET microscopic imaging in single living cells on a wide-field microscope by combining the spatial filtering character of LCTF and the imaging function of wide-field microscope. Compared with confocal microscopic system, the spectral wide-field microscopic imaging system reduced the cost from about 350,000 dollars to about 50,000 dollars. Moreover, the spectral wide-field microscopic imaging system is very stable from every starting up to at least 3 months, while confocal microscope must be calibrated for every power-on. Therefore, we can directly implement FRET quantification measurement on the spectral wide-field microscopic imaging system without calibration for at least 3 months once the system was precalibrated, which greatly improves research efficiency due to the circumvention of additional reference samples or complex calibration procedure in every measurement. Additionally, we can flexibly install filters or transform light paths in wide-field microscope to meet more demands. Because of a small size of  $8.5 \times 5 \times 5 \text{ cm}^3$  and a common USB line, the portable LCTF can be easily integrated to a wide-field microscope

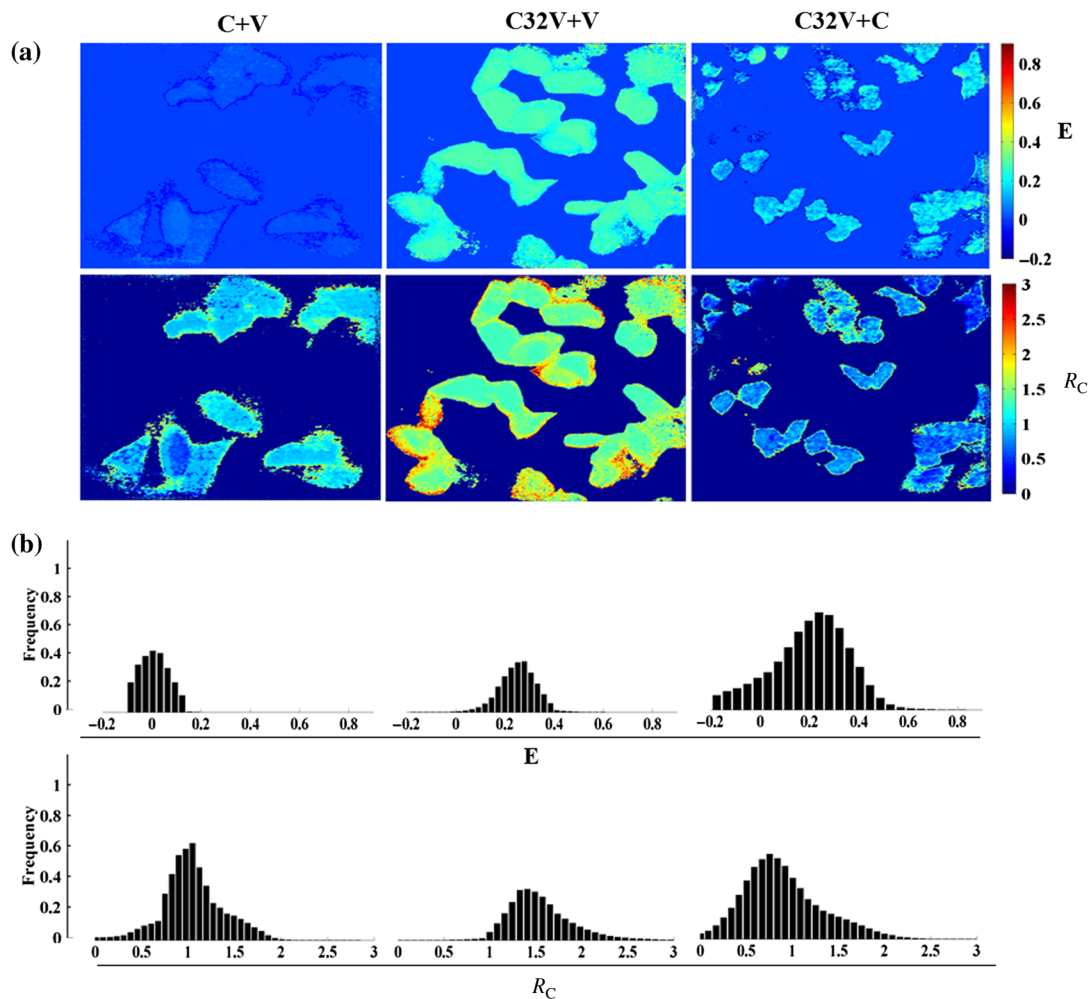


**Fig. 5** Quantification of FRET constructs in the presence of free donors and acceptors. (a)  $E$  and  $R_C$  images of living HepG2 cells expressing C+V, C32V+V and C32V+C, respectively. (b) Histograms of  $E$  and  $R_C$  corresponding to (a).

with detachable standard C ports and electric controlled with open software developer's kit, which would largely extend the live-cell application of FRET technology, especially FRET imaging for subcellular localization or dynamic protein-protein interaction in living cells. The Varispec LCTF family includes six models with different wavelength scanning ranges and different bandwidths (FWHM), and the total wavelength range covers 400 to 2450 nm, the narrowest FWHM is 0.25 nm, and the widest FWHM is 20 nm. Note that the FWHM could not be changed for a specific LCTF model, such as the LCTF we used has a fixed FWHM of 10 nm and a wavelength range of 400 to 720 nm.

### 3.4 Fluorescence Resonance Energy Transfer Imaging in the Presence of Free Donors and Acceptors

We next implemented Iem-spFRET method on our spectral wide-field microscopic FRET imaging system for the living HepG2 cells coexpressing free Cerulean(C) and free Venus-Kras(V), C32V and free V as well C32V and free C, respectively. As we can see from Fig. 5, cells expressing C+V exhibited  $\sim 0$  of  $E$  and  $\sim 1.15$  of  $R_C$  with very variable distributions, cells expressing C32V+V exhibited 29% of  $E$  with a narrow distribution and  $\sim 1.40$  of  $R_C$  with very variable distribution, and cells expressing C32V+C exhibited  $\sim 23\%$  of  $E$  and  $\sim 0.75$  of  $R_C$  with very variable distributions.

The  $E$  values of cells expressing C32V+V and C32V is comparable, whereas the  $R_C$  values of cells expressing C32V+V are larger than those of cells expressing C32V alone [Fig. 5, second column and Figs. 4(c) and 4(d), first column]. However, both  $R_C$  and  $E$  values of cells expressing C32V+C were reduced compared to the  $R_C$  and  $E$  values of cells expressing C32V alone [Fig. 5, last column and Figs. 4(c) and 4(d), first column]. Moreover, pseudocolor images and histograms showed no FRET and a variable distribution of  $R_C$  for C+V sample, a restricted distribution of  $E$  values but a variable distribution of  $R_C$  for C32V+V sample, and variable distributions of both  $E$  and  $R_C$  for C32V+C sample (Fig. 5). Similar results have been reported in recent publications.<sup>12,17</sup> In fact, in the presence of free donor and/or acceptor, the  $E$  value we measured is the apparent FRET efficiency normalized to donor concentration.<sup>22</sup> Therefore, it is reasonable that the  $E$  values did not change in the presence of free acceptor (V) but decreased in the presence of free donor (C) with an inversely proportional relation to the free donor fraction. The  $R_C$  that we measured is the total concentration ratio of acceptor to donor, so it should decrease in the presence of free donors but increase in the presence of free acceptors. In addition, from samples expressing unlinked Venus, C+V, and C32V+V, we can find two facts: (1) cellular outlines exhibit larger  $R_C$  values [Fig. 5(a), bottom row, first two columns], which is resulted from the fact that Venus-Kras is a membrane protein; but (2) their  $E$  images presented almost uniform values in cells [Fig. 5(a), top row, first two columns], which is owed to effective subtraction of the acceptor excitation crosstalk, a key issue for quantitative FRET measurement,<sup>22</sup> from the total acceptor emission in Iem-spFRET approach.

## 4 Conclusions

In this report, we set up a spectral wide-field microscopic FRET imaging system by integrating a LCTF into a wide-field microscope. Our system can be used to implement all emission-spectral unmixing FRET imaging. Moreover, this platform can

be also developed to implement recently arisen ExEm unmixing-based imaging and multicolor FRET imaging. This stable and low-cost spectral wide-field microscopic FRET imaging system provides a new toolbox for imaging intracellular molecular processes with high spatial resolution in living cells, which would largely extend the live-cell application of FRET technology.

### Acknowledgments

The authors thank Prof. S.S. Vogel (NIH/NIAAA) for providing C32V, CVC, VCV, and VCVV plasmids. This work is supported by the National Natural Science Foundation of China (NSFC) (Grant No. 81471699) and in part by the National Key Basic Research Program of China (Grant No. 2015CB352006) as well as the Science and Technology Plan Project of Guangdong Province in China (Grant No. 2014B090901060).

### References

1. J. R. Lakowicz, *Principles of Fluorescence Spectroscopy*, 3rd ed., Springer, Singapore (2006).
2. I. L. Medintz, "Recent progress in developing FRET-based intracellular sensors for the detection of small molecule nutrients and ligands," *Trends. Biotechnol.* **24**(12), 539–542 (2006).
3. L. Stryer, "Fluorescence energy transfer as a spectroscopic ruler," *Ann. Rev. Biochem.* **47**, 819–846 (1978).
4. Á. I. Fábán et al., "Strength in numbers: effects of acceptor abundance on FRET efficiency," *ChemPhysChem.* **11**, 3713–3721 (2010).
5. L. L. Zhang et al., "Binomial distribution-based quantitative measurement of multiple-acceptors fluorescence resonance energy transfer by partially photobleaching acceptor," *Appl. Phys. Lett.* **104**(24), 243706 (2014).
6. M. Mohsin et al., "Genetically encoded FRET-based nanosensor for in vivo measurement of leucine," *Biosens. Bioelectron.* **50**, 72–77 (2013).
7. E. A. Jares-Erijman and T. M. Jovin, "FRET imaging," *Nat. Biotechnol.* **21**(11) 1387–1395 (2003).
8. E. A. Jares-Erijman and T. M. Jovin, "Imaging molecular interactions in living cells by FRET microscopy," *Curr. Opin. Chem. Biol.* **10**, 409–416 (2006).
9. T. Zal and N. R. J. Gascoigne, "Photobleaching-corrected FRET efficiency imaging of live cells," *Biophys. J.* **86**(6), 3923–3939 (2004).
10. H. Chen et al., "Measurements of FRET efficiency and ratio of donor to acceptor concentration in living cells," *Biophys. J.* **91**(5), L39–L41 (2006).
11. L. Chai et al., "Miniature fiber optic spectrometer-based quantitative fluorescence resonance energy transfer measurement in single living cells," *J. Biomed. Opt.* **20**(3), 037008 (2015).
12. S. Levy et al., "SpRET: highly sensitive and reliable spectral measurement of absolute FRET efficiency," *Microsc. Microanal.* **17**, 176–190 (2011).
13. A. D. Hoppe et al., "N-way FRET microscopy of multiple protein-protein interactions in live cells," *PLoS One* **8**(6), e64760 (2013).
14. A. Woehler, "Simultaneous quantitative live cell imaging of multiple FRET-based biosensors," *PLoS One* **8**(4), e61096 (2013).
15. C. Thaler et al., "Quantitative multiphoton spectral imaging and its use for measuring resonance energy transfer," *Biophys. J.* **89**(4), 2736–2749 (2005).
16. J. Włodarczyk et al., "Analysis of FRET signals in the presence of free donors and acceptors," *Biophys. J.* **94**, 986–1000 (2008).
17. J. Zhang et al., "Quantitative FRET measurement using emission-spectral unmixing with independent excitation crosstalk correction," *J. Microsc.* **257**(2), 104–116 (2015).
18. S. Mustafa et al., "Quantitative Förster resonance energy transfer efficiency measurements using simultaneous spectral unmixing of excitation and emission spectra," *J. Biomed. Opt.* **18**(2), 026024 (2013).
19. M. Elangovana et al., "Characterization of one- and two-photon excitation fluorescence resonance energy transfer microscopy," *Methods* **29**(1), 58–73 (2003).

20. Y. Chen and A. Periasamy, "Intensity range based quantitative FRET data analysis to localize protein molecules in live cell nuclei," *J. Fluoresc.* **16**(1), 95–104 (2006).
  21. H. Yu, T. Chen, and J. Qu, "Improving FRET efficiency measurement in confocal microscopy imaging," *Chin. Opt. Lett.* **8**(10), 947–949 (2010).
  22. A. D. Elder et al., "A quantitative protocol for dynamic measurements of protein interactions by Förster resonance energy transfer-sensitized fluorescence emission," *J. R. Soc. Interface* **6**(S1), S59–S81 (2009).
  23. L. X. Wang et al., "Photobleaching-based quantitative analysis of fluorescence resonance energy transfer inside single living cell," *J. Fluoresc.* **20**(1), 27–35 (2010).
  24. H. L. Li, H. N. Yu, and T. S. Chen, "Partial acceptor photobleaching-based quantitative FRET method completely overcoming emission spectral crosstalks," *Microsc. Microanal.* **18**(5), 1021 (2012).
  25. H. N. Yu et al., "An empirical quantitative fluorescence resonance energy transfer method for multiple acceptors based on partial acceptor photobleaching," *Appl. Phys. Lett.* **100**, 253701 (2012).
  26. H. N. Yu et al., "Ma-PbFRET: multiple acceptors FRET measurement based on partial acceptor photobleaching," *Microsc. Microanal.* **19**(1), 171 (2013).
  27. S. V. Koushik, P. S. Blank, and S. S. Vogel, "Anomalous surplus energy transfer observed with multiple FRET acceptors," *PLoS One* **4**(11), e8031 (2009).
  28. G. Patterson, R. N. Day, and D. Piston, "Fluorescent protein spectra," *J. Cell Sci.* **114**(5), 837–838 (2001).
  29. M. A. Rizzo et al., "An improved cyan fluorescent protein variant useful for FRET," *Nat. Biotechnol.* **22**, 445–449 (2004).
  30. T. Nagai et al., "A variant of yellow fluorescent protein with fast and efficient maturation for cell-biological applications," *Nat. Biotechnol.* **20**, 87–90 (2002).
  31. S. V. Koushik and S. S. Vogel, "Energy migration alters the fluorescence lifetime of Cerulean: implications for fluorescence lifetime imaging Förster resonance energy transfer measurements," *J. Biomed. Opt.* **13**(3), 031204 (2008).
  32. H. R. Morris, C. C. Hoyt, and P. J. Treado, "Imaging spectroscopy for fluorescence and Raman microscopy, acousto-optic and liquid crystal tunable filters," *Appl. Spectrosc.* **48**, 857–870 (1994).
  33. R. Lansford, G. Bearman, and S. E. Fraser, "Resolution of multiple green fluorescent protein color variants and dyes using two-photon microscopy and imaging spectroscopy," *J. Biomed. Opt.* **6**(3), 311–318 (2001).
  34. PCO Company Website, <http://www.pco.de/> (12 August 2015).
  35. VariSpec Liquid Crystal Tunable Filters (Data Sheet), [http://www.perkinelmer.com/CMSResources/Images/44-140156DTS\\_010053A\\_01\\_VariSpec\\_DTS.pdf](http://www.perkinelmer.com/CMSResources/Images/44-140156DTS_010053A_01_VariSpec_DTS.pdf), 2013 (12 August 2015).
- Lili Zhang** received her BS in physics from Hubei University, China. She is the author of four journal papers. Her current research interests include fluorescence microscopy and biomedical optics.
- Guiqi Qin** received his master's degree in South China Normal University. He is the author of six journal papers.
- Liuying Chai** received her master's degree in South China Normal University. She is the author of four journal papers. She is studying for a doctor's degree in Shanghai Jiao Tong University.
- Jiang Zhang** is studying for his master's degree in South China Normal University. His current research interests include quantitative FRET imaging.
- Fangfang Yang** is studying for her master's degree in South China Normal University. Her current research interests include biomedical applications of FRET imaging.
- Hongqin Yang** is the professor in the college of photonic and electronic Engineering, Fujian Normal University. His research interests include biomedical optics.
- Shusen Xie** is the professor in the college of photonic and electronic Engineering, Fujian Normal University. He is a discipline leader of biomedical optics in China.
- Tongsheng Chen** received his PhD in biomedical engineering from the Huazhong University of Science and Technology, China. He has 15 years of experience in fluorescence microscopy and biomedical optics. Since 2005, he has been a full professor of the MOE Key Laboratory of Laser Life Science & Institute of Laser Life Science; South China Normal University, Guangzhou, China. He is the author of more than 100 journal papers, and he is also a member of SPIE.